

# Synthesis of higher-order Poincaré sphere THz beams

YAQUN LIU\*, VALDAS PASISKEVICIUS

Department of Applied Physics, Royal Institute of Technology, Roslagstullsbacken 21, 106 91 Stockholm, Sweden

\*[yaqun@kth.se](mailto:yaqun@kth.se)

A novel method to generate vector vortex THz beams with angular momentum by a pair of pumps was reported. The helicity of the vector THz beam, that from polarization to orbital angular momentum can be finely tuned by manipulating the pulse delay between two pump pulses and a S-waveplate. All the states of THz vector vortices on the higher-order Poincaré sphere are able to be generated. The synthesis was theoretically explored and experimentally verified. This approach paves the way to the sources of versatile structured THz beams and may benefit the potential applications.

## Introduction

Terahertz (THz) attracts great interest for broad applications in spectroscopy, imaging, sensing, and communication [1-3]. Vortex beams carry orbital angular momentum and have associated embedded wavefront phase singularities (scalar vortex beams) or polarization singularities (vector vortex beams). The complex vector vortex THz beams, which carry both orbital angular momentum (OAM) and spin angular momentum (SAM), like circularly polarized vortex THz, provide additional tools for applications in the next generation of wireless communications, spectroscopy, and manipulation of novel magnetic and chiral materials [4-8].

A light field possesses two common types of helicity [9]. One helicity is a local property, and determined by the local polarization within a beam. This helicity is, obviously, related to the existence of spin angular momentum (SAM),  $S = \pm\hbar$  (right handedness:  $S = -\hbar$ , left handedness:  $S = +\hbar$ , corresponding to the clockwise and anticlockwise motion, respectively, defined from the observer point of view). The other helicity is a global spatial property, related to the spiral structure of the azimuthal phase or polarization. Orbital angular momentum (OAM)  $L = l\hbar$  parametrizes the global helicity of the beam. Integer  $l$  is the topological winding number, the absolute value of which represents how many times of  $2\pi$  the azimuthal phase/polarization acquires. As in the case of spin, the sign of  $l$  represents the left handedness ( $l > 0$ ) and right handedness ( $l < 0$ ). The light beam that possesses both types of helicity is referred to as the complex vector vortex. The higher-order Poincaré (HOP) sphere construct was defined to describe the states of polarization (SOP) of the complex vector vortex beams with both SAM and OAM [10-12]. To be consistent with the validation experiment in this work, the order of  $|l| = 2$  is employed. The polarization and phase distributions of vector vortex

beams on HOP sphere are shown in Fig. 1. The beams on equator have spiral linear polarization structure which is known as cylinder vortex (CV) beams [13]. The poles on the sphere represent circular polarized vortices with opposite handedness. On the North pole it represents right circular vortex, while on South pole it is left circular vortex. Other beams on the sphere are complex structured vortices with non-uniform elliptical local polarization.

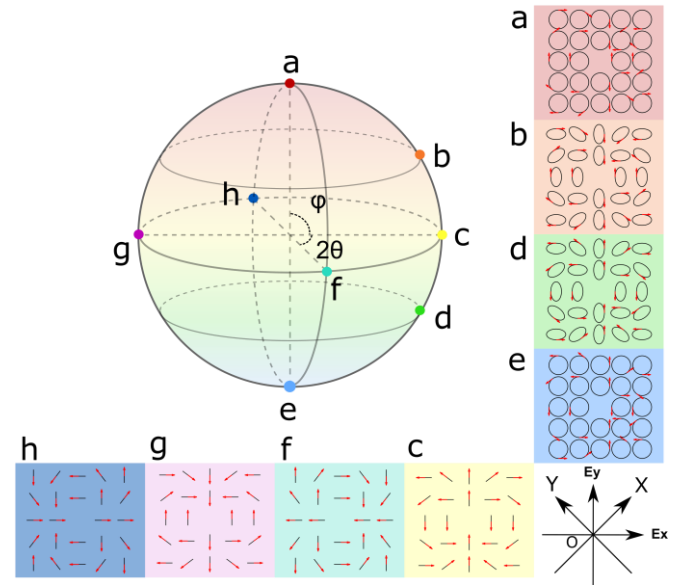


Fig. 1. Scheme of higher-order Poincaré sphere corresponding to  $||=2$ . The insets represent SOP of the vector vortex beams. **a**: right-hand circular polarized in red, **b**: right-hand elliptical polarized in orange, **d**: left-hand elliptical polarized in green, **e**: left-hand circular polarized in light blue, **c**, **f**, **g** and **h**: linear polarized on the equator (in yellow, cyan, purple and navy).

As one of the commonly used THz generation methods, optical rectification (OR) ensures automatic temporal phase stability, making it well-suited for THz field synthesis. Circular polarization THz radiation generation was reported with two phase-delayed pumps in 110-crystal like ZnTe and Bi<sub>4</sub>Ge<sub>3</sub>O<sub>12</sub> [14,15]. However, this scheme requires the specific angle between two linearly polarized pumps and their relative placement with the crystal, that prevents the potential of generating the circularly polarized vortex THz beams with both OAM and SAM. Recently, vector and

scalar vortex THz were generated in 111-ZnTe by employing pump with polarization singularity [16,17]. The high symmetry of three-fold symmetric axis of zinc-blende nonlinear crystal also breaks the limitation of specific scheme requirements as in 110-crystal, enables the generation of the complex vector vortex THz fields. Thus, OR along the three-fold symmetric axis of zinc-blende nonlinear crystal is chosen due to insensitivity of the nonlinearity with respect to the pump polarization to guarantee the local and global helicity at the same time.

In this work we demonstrate synthesis of THz complex vector vortex beams on HOP sphere by two phase delayed near-IR pump beams along the three-fold symmetric axis of zinc-blende nonlinear crystal. The pumps are shaped to be CV beams using nanostructured silica S-waveplate [18] that provides quasi-continuous spatial birefringence distribution and is suitable for power scaling. The pulse delay between pump beams and the rotation angle of S-waveplate provide the degree of freedom to traverse the entire HOP sphere with the generated THz field states. The angular momentum and the state of polarization of complex THz beams are derived from different pump fields with controllable pulse delay.

The polarization of synthesized vector vortex THz beam in reconstruction coordinate frames (see **Supplementary Information**) can be described by

$$P = \left[ \cos\left(\frac{\varphi}{2} + \frac{\pi}{4}\right) e^{(+i2\phi - \frac{\pi}{2} - 2\theta)} \right] \left| L \right\rangle + \left[ \sin\left(\frac{\varphi}{2} + \frac{\pi}{4}\right) e^{(-i2\phi - \frac{\pi}{2} - 2\theta)} \right] \left| R \right\rangle$$

Where,  $\phi$  represents the azimuthal angle, is the general phase delay between the pump beams,  $\theta$  is the S-waveplate angle.

## Experiment

The generation of different vectorial THz vortices were experimentally demonstrated by employing a 111-ZnTe. The scheme of THz generation by dual pump pulses is illustrated in Fig. 2(a). The two pump pulses are synchronized with a delay ranging in hundreds of fs, of which the value depends on the target frequency. For example, a phase delay of  $\pi/2$  at 1 THz corresponding to a time delay of 250 fs. The time interval of the pulse train is 1 ms, arising from the repetition rate of pump laser of 1 kHz. The generated THz radiation is few-cycled that the pulse duration is in several ps, determined by the nonlinear crystal length and pump laser

parameters. The pulse duration of IR pump used in this work is 33 fs. The scheme of local THz field polarization and handedness are shown in Fig. 2(a). A simulated temporal THz waveform which is shown in red in Fig. 2(a), is calculated using a 1.5mm nonlinear ZnTe crystal by a 150-fs pump laser operating at 800 nm with the consideration of phase mismatch and absorption. An additional phase delay  $\varphi$  was applied onto the phase term by working on the Fourier transform of this original THz temporal signal to get a phase delayed THz signal. The phase delayed temporal THz waveform with  $\varphi = \pi/2$ , is illustrated in blue in Fig. 2 (a) by another Fourier transform conversion. The original and the phase delayed THz signal are set as horizontal and vertical polarized. The trajectory of the superposed generated THz waveform is illustrated in Fig. 2(a)-ii, exhibiting right circular polarization. Akin to this, the THz signal will be left circular polarized with the phase delay of  $-\pi/2$ .

The schematic experimental set-up is illustrated in Fig.2 (b). Horizontally linearly polarized laser with a central wavelength of 800 nm, a pulse duration of 33 fs, repetition rate of 1 kHz (Astrella, Coherence), was used as pump and probe beam. The pump beam was further split into two beams - Pump 1 and Pump 2. The Pump 2 maintained horizontally polarized. A half waveplate and a polarizer were employed onto Pump 1 to control the polarization orientation and power. The two pump beams are  $45^\circ$  linearly polarized with each other with balanced power of 30 mW and spatial overlap. The power of probe beam used in this paper was 6 mW as dictated by the CCD camera properties. A delayline was applied onto Pump 2 to manipulate the pulse delay between two pump beams. The zero-phase delay was calibrated by using another delay-line on probe beam arm together (see **Methods**). An S-waveplate was inserted before the nonlinear crystal ZnTe to convert the two linear polarized pumps into two CV pump beams. Vector vortices of THz signal with a doubling TC were generated using a 111-ZnTe crystal. The schematic transformations of SOPs of pumps and THz beams generated independently by each pump are described in **Methods**. Two 4f systems with a total demagnification of 4 were built for THz imaging. The THz electric field distribution was captured by a synchronized charge-coupled device (CCD) using the dynamic subtraction technique [19] based on electric-optic sampling (EOS) using a 110-ZnTe crystal. THz polarimetry technique (see **Methods**) was employed to measure the THz electric field components  $E_x$  and  $E_y$ , separately. The trajectory of THz waveform is thus reconstructed to obtain polarization.

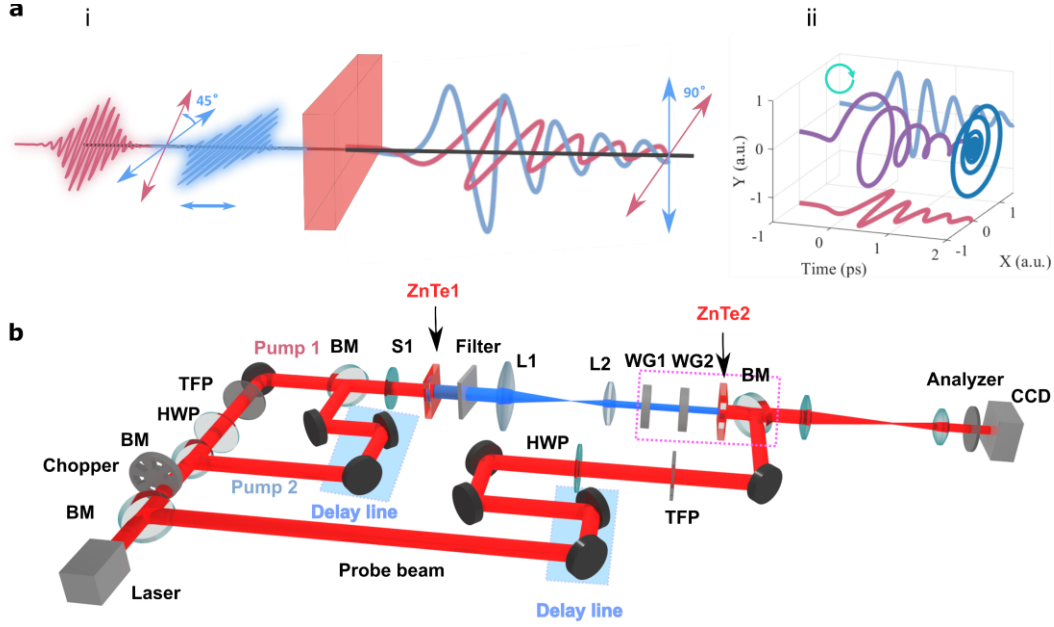


Fig. 2. Scheme of local THz generation by dual pumps (a) and experimental set-up (b). (a)-i, dual fs pump pulses are in red (at a phase of 0) and blue (at a phase of  $\pi/2$ ). Arrows: represent polarization orientation; ii, THz trajectory with right circular polarization; purple: waveform trajectory, Navy: waveform projection, red and blue: two perpendicular THz electric field components, cyan circle arrows: handedness. (b) Experimental set-up. BM: beamsplitter, HWP: half waveplate, TFP: thin film polarizer, S1: S-waveplate, ZnTe1: 111-ZnTe, ZnTe2: 110-ZnTe. WG1, WG2: wire grid polarizer.

## Results

Five typical states of complex vector THz vortices illustrated on a meridian in Fig. 1 a-e are generated by manipulating the phase delay between two pumps with S-waveplate setting at  $0^\circ$ . The experimental results are measured and characterized to prove the validity and feasibility of this scheme.

A phase delay of  $\pi/2$  was set by adjusting the delay-line in Pump 2 arm as shown in Fig. 2(b). To implement the reconstruction of THz field, the decomposition into two orthogonal eigenstates in the linear polarization basis -  $E_x$  and  $E_y$  was introduced, of which the orientations are shown in **Methods**. To visualize the evolution of THz field, the temporal electrical field distributions of  $E_x$  and  $E_y$  were imaged in a range of 1.6 mm, with a step of 0.01 mm, that in the time range of 5.3 ps with a resolution of 33 fs, separately. Fourier transform was subsequently employed to map the amplitude and phase distributions of these two eigenstates. The amplitude and phase distributions of  $E_y$  at 0.95 THz are shown in Fig. 3(a) and (c), while that of  $E_x$  are shown in Fig. 3(b) and (d). The spiral phases depicted in Fig. 3(c) and (d) both exhibit an anticlockwise of  $4\pi$  indicating the presence of OAM of  $-2\hbar$ . These two eigenstates are revealed to be two scalar vortex beams with the same topological charge (TC) of -2. The simulated reconstructed SOP of the THz field is shown in Fig. 3(e). A typical experimental reconstructed 3D THz local waveform trajectory and projection of the beam position at [0.9 mm, 0.9 mm] are shown in Fig. 3(f), corresponding to the simulated trajectory marked in red in Fig. 3(e). The handedness in the figure confirms the right-handedness, which is marked in Cyan circle in Fig. 3(f), exhibiting the SAM of  $-\hbar$ . Note that the handedness of the experimental

results demonstrated in this work are from the point of view of the observer. This beam corresponds to the SOP of Fig. 1-a on the North pole illustrated in light red.

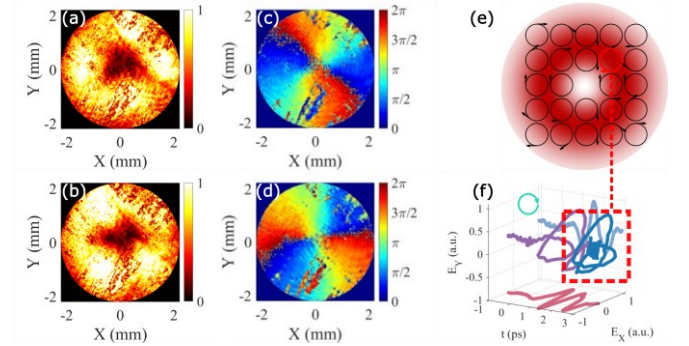
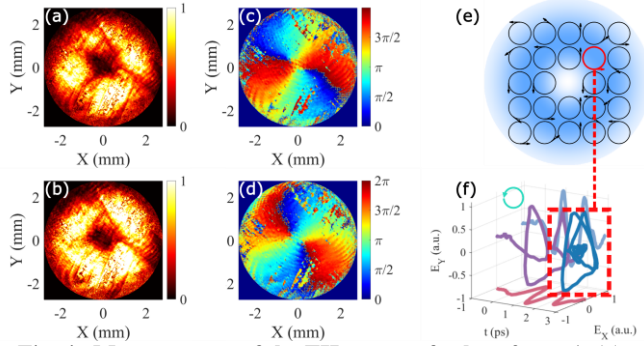


Fig. 3. Measurement of the THz vortex for  $l = -2$ ,  $s = -1$ . (a), THz electric field amplitude distribution along  $E_y$  axis. (b), Amplitude distribution along  $E_x$  axis. (c), Phase distribution along  $E_y$  axis. (d), Phase distribution along  $E_x$  axis. Color bars in (a) and (b) show the intensities in arbitrary units, and color bars in (c) and (d) represent the phase scale (radian). (e), Simulated trajectory of THz temporal waveform. (f), measured trajectory of local THz temporal waveform (the position labelled red in SOP (e)).

By controlling the pulse delay between the pump beams, the polarization helicity of the vortex beam can be flipped from the right-circular to left-circular polarization. Fig. 4 shows the experimental results of two eigenstates of the left circular polarized THz vortex, corresponding to the South pole SOP in Fig. 1. Similar to the first case, the measured 3D electric field trajectory of the same position is shown in Fig. 4(f), confirming the left-handedness. This handedness exhibits the SAM of  $+\hbar$ . The phase delay not only reverses the

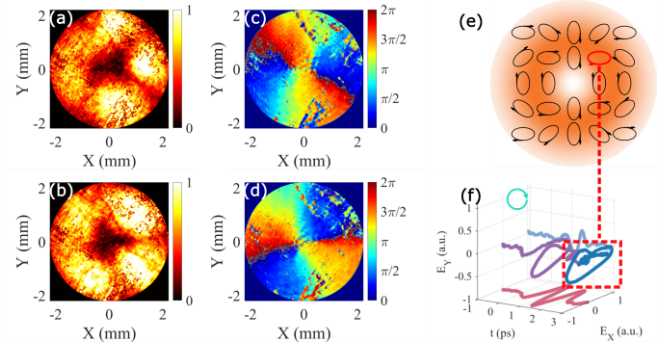
handedness of the circular polarization, as should be expected, but also flips the sign of TC. The phases in Fig 4. (c) and (d) both show an  $4\pi$  clockwise spiral feature, indicating an OAM of  $+2h$ .



**Fig. 4. Measurement of the THz vortex for  $l = +2$ ,  $s = +1$ .** (a), THz electric field amplitude distribution along  $E_y$  axis. (b), Amplitude distribution along  $E_x$  axis. (c), Phase distribution along  $E_y$  axis. (d), Phase distribution along  $E_x$  axis. Color bars in (a) and (b) show the intensities in arbitrary units, and color bars in (c) and (d) represent the phase scale (radian). (e), Simulated trajectory of THz temporal waveform. (f), measured trajectory of local THz temporal waveform (the position labelled red in SOP (e)).

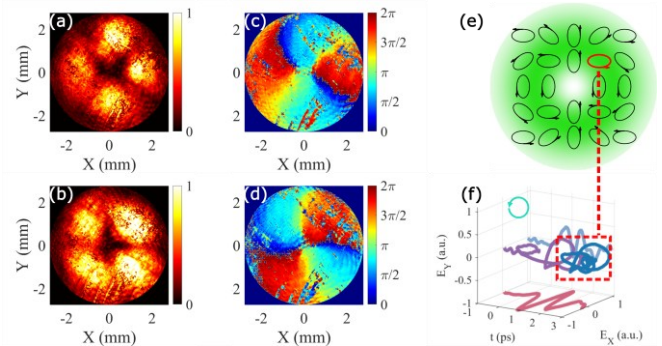
The local polarization can be controlled between circular, elliptical, and linear polarization depending on the pulse phase delay between two pump beams. Among all the beams, the general case is the vortex beam with local elliptically polarizations. The vortex beams with right and left elliptically polarization, of which the SOPs are plotted in orange and green on the HOP in Fig. 1, were also generated and characterized.

The experimental results of THz vortex beam were measured while the phase delay was set as  $\pi/4$  as shown in Fig. 5. The evolutions of wavefront of the two eigenstates in 1.65 ps (50 frames) are shown in the attached videos (Fig. 5\_Ex.mp4 and Fig. 5\_Ey.mp4). They both exhibit the counterclockwise rotation, and the phase distributions in Fig. 5(c) and (d) verify a TC of  $-2$ . However, the amplitude profiles in Fig. 5(a) and (b) are not as uniform as that in Fig. 3 and Fig. 4. This un-uniform results from the local elliptical polarization. The amplitude of  $E_y$  in Fig. 5(a) has maximum values along horizontal and vertical directions through the beam center, while the  $E_x$  amplitude in Fig. 5(b) has minimum value along horizontal and vertical directions. The un-uniform feature is consistent with the SOP shown in Fig. 5(e) as we expected. For the local elliptical polarizations that along horizontal and vertical directions through the beam center, the long axis is along  $E_y$  while the short axis of that is along  $E_x$ . The measured THz trajectory in Fig. 5(f) corresponds with the simulated in red in Fig. 5(e), that are right-handed and elliptically polarized with long axis along  $E_x$ . As a general beam on the HOP sphere, it further verifies the experimental agreement to the simulation and theory.



**Fig. 5. Measurement of right-handed elliptical THz vortex beam.** (a), THz electric field amplitude distribution along  $E_y$  axis. (b), Amplitude distribution along  $E_x$  axis. (c), Phase distribution along  $E_y$  axis. (d), Phase distribution along  $E_x$  axis. Color bars in (a) and (b) show the intensities in arbitrary units, and color bars in (c) and (d) represent the phase scale (radian). (e), Simulated trajectory of THz temporal waveform. (f), measured trajectory of local THz temporal waveform (the position labelled red in SOP (e)).

Similarly, the experimental results of THz vortex beam while the phase delay was set as  $-\pi/4$  are shown in Fig. 6. The amplitude distributions in Fig. 6(a) and (b) start to show an inclination to the four-lobe feature of CV beams, which is the interposition between a CV and circular polarization vortex. The  $E_y$  has maximum values amplitudes along horizontal and vertical directions, while  $E_x$  has minimum amplitudes along them. The evolutions of wavefront of the two eigenstates in 1.65 ps (50 frames) are also attached in videos (Fig. 6\_Ex.mp4 and Fig. 6\_Ey.mp4). In this case, they both exhibit the counterclockwise rotation which implies the TC of  $+2$  with the consideration of the phase distributions in Fig. 6(c) and (d). The 3D reconstructed THz electric field trace in Fig. 6(f) demonstrates the left-handed elliptical polarization with long axis along  $E_x$  axis.

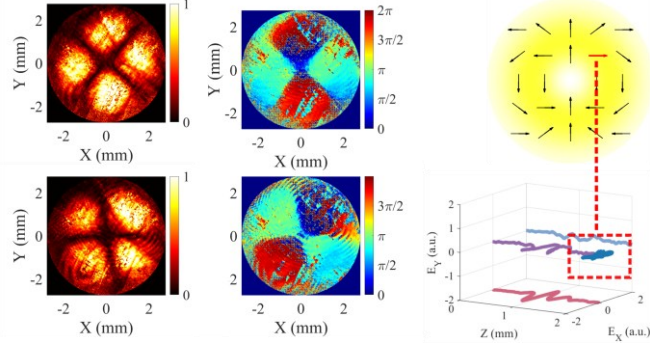


**Fig. 6. Measurement of left-handed elliptical THz vortex beam.** (a), THz electric field amplitude distribution along  $E_y$  axis. (b), Amplitude distribution along  $E_x$  axis. (c), Phase distribution along  $E_y$  axis. (d), Phase distribution along  $E_x$  axis. Color bars in (a) and (b) show the intensities in arbitrary units, and color bars in (c) and (d) represent the phase scale (radian). (e), Simulated trajectory of THz temporal waveform. (f), measured trajectory of local THz temporal waveform (the position labelled red in SOP (e)).

The phase and amplitude of the CV THz beam with zero phase delay between pumps was also measured and



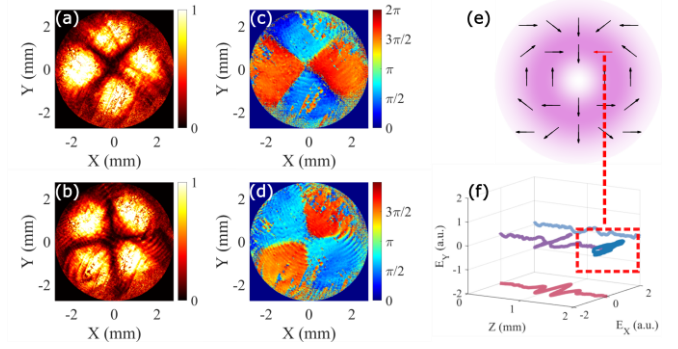
reconstructed to verify that the transformation along the meridian is valid. The experimental results of the CV THz beam are illustrated in Fig. 7. The amplitudes in Fig. 7(a) and (b) exhibit the clear four-petal feature, with the phases between two lobes has a  $\pi$  shift. This verifies the CV beam structure. The measured trajectory of THz waveform shows a linear polarization along  $E_x$  axis, that satisfies with the SOP simulated in Fig. 7(e). This beam corresponds to the CV beam represented by state c on the equator in Fig. 1. The consistency between simulation and experimental results confirms the correctness of the reconstructed experimental circular and elliptical polarized THz vortex results shown above.



**Fig. 7. Measurement of CV THz beam with S-waveplate at  $0^\circ$ .**

(a), THz electric field amplitude distribution along  $E_y$  axis. (b), Amplitude distribution along  $E_x$  axis. (c), Phase distribution along  $E_y$  axis. (d), Phase distribution along  $E_x$  axis. Color bars in (a) and (b) show the intensities in arbitrary units, and color bars in (c) and (d) represent the phase scale (radian). (e), Simulated trajectory of THz temporal waveform. (f), measured trajectory of local THz temporal waveform (the position labelled red in SOP (e)).

To further verify another manipulating degree of freedom-rotation angle of S-waveplate, another state on the equator was generated by rotating the S-waveplate from  $0^\circ$  to  $90^\circ$ , with phase delay remaining as zero. The amplitude and phase of this CV THz beam was shown in Fig. 8(a)-(d), exhibiting the same four-petal feature as Fig. 7(a)-(d). The 3D trace was also reconstructed in Fig. 8(f), corresponding to the local polarization labelled in red in Fig. 8(e). This CV beam agrees well with the SOP of Fig.1-g, as we expected. The vector vortex THz beams at the equator have been verified to transform via S-waveplate rotation, confirming that THz vortex beams at the same latitude can be correctly generated by rotating S-waveplate, as predicted by our theory. By adjusting the pulse delay between pumps and the rotation angle of the S-waveplate as two degrees of freedom, THz beams with six different SOPs on HOP sphere were generated and measured thoroughly.



**Fig. 8. Measurement of CV THz beam with S-waveplate at  $90^\circ$ .**

(a), THz electric field amplitude distribution along  $E_y$  axis. (b), Amplitude distribution along  $E_x$  axis. (c), Phase distribution along  $E_y$  axis. (d), Phase distribution along  $E_x$  axis. Color bars in (a) and (b) show the intensities in arbitrary units, and color bars in (c) and (d) represent the phase scale (radian). (e), Simulated trajectory of THz temporal waveform. (f), measured trajectory of local THz temporal waveform (the position labelled red in SOP (e)).

## Conclusion

In conclusion, we theoretically explored and experimentally demonstrated a simple synthesis approach to generate vector-vortex THz beams directly through optical rectification in a three-fold symmetric nonlinear crystal, using two infrared pump beams. By manipulating the time delay between two pump pulses and the S-waveplate rotation angle, the helicity of THz beam was tuned to map all the complex vector vortex beams on HOP sphere. We successfully generated and characterized linear, left and right circular, and elliptical polarization vector THz vortices by a THz imaging system. The excellent agreement between the theoretical and the experimental beam profile verifies the validity of our method for arbitrary polarization-shaped vortex THz beams generation. This method provides a simple way to produce complex vector beams in THz, broadening their further applications.

## References

- [1] Tonouchi, M. Cutting-edge terahertz technology. *Nature Photon* 1, 97–105 (2007).
- [2] F. Hindle, R. Bocquet, A. Pienkina, A. Cuisset, and G. Mouret, "Terahertz gas phase spectroscopy using a high-finesse Fabry–Pérot cavity," *Optica* 6 (2019).
- [3] Nagatsuma, T., Ducournau, G. & Renaud, C. Advances in terahertz communications accelerated by photonics. *Nature Photon* 10, 371–379 (2016).
- [4] Minagawa, H., Yoshimura, S., Terasaka, K. et al. Enhancement of Doppler spectroscopy to transverse direction by using optical vortex. *Sci Rep* 13, 15400 (2023).
- [5] Jepsen, P. U., Cooke, D. G. & Koch, M. Terahertz spectroscopy and imaging-Modern techniques and applications. *Laser Photon Rev.* 5,124–166 (2011).
- [6] Barreiro, J., Wei, TC. & Kwiat, P. Beating the channel capacity limit for linear photonic superdense coding. *Nature Phys* 4, 282–286 (2008).

- [7] Molina-Terriza, G., Torres, J. P. & Torner, L. Twisted photons. *Nat. Phys.* 3, 305–310 (2007).
- [8] Basini, M., Pancaldi, M., Wehinger, B. et al. Terahertz electric-field-driven dynamical multiferroicity in SrTiO<sub>3</sub>. *Nature* 628, 534–539 (2024).
- [9] Bliokh, K., Rodríguez-Fortuño, F., Nori, F. et al. Spin-orbit interactions of light. *Nature Photon* 9, 796–808 (2015). <https://doi.org/10.1038/nphoton.2015.201>.
- [10] Naidoo, D., Roux, F., Dudley, A. et al. Controlled generation of higher-order Poincaré sphere beams from a laser. *Nature Photon* 10, 327–332 (2016).
- [11] Milione, G., Sztul, H. I., Nolan, D. A. & Alfano, R. R. Higher-order Poincaré sphere, Stokes parameters, and the angular momentum of light. *Phys. Rev. Lett.* 107, 053601 (2011).
- [12] Milione, G., Evans, S., Nolan, D. A. & Alfano, R. R. Higher-order Pancharatnam–Berry phase and the angular momentum of light. *Phys. Rev. Lett.* 108, 190401 (2012).
- [13] Qiwen Zhan, Cylindrical vector beams: from mathematical concepts to applications, *Adv. Opt. Photon.* 1, 1-57 (2009).
- [14] Shimano, Ryo, Hisaaki Nishimura, and Tomohiro Sato. "Frequency tunable circular polarization control of terahertz radiation." *Japanese journal of applied physics* 44.5L (2005): L676.
- [15] Takeda, R., et al. "Circularly polarized narrowband terahertz radiation from a eulytite oxide by a pair of femtosecond laser pulses." *Physical Review A* 89.3 (2014): 033832.
- [16] Yaqun Liu, Valdas Pasiskevicius; Generation of THz vector and scalar vortex beams by optical rectification along threefold symmetry axis in zinc blende crystals. *APL Photonics* 1 April 2025; 10 (4): 046101. <https://doi.org/10.1063/5.0254769>.
- [17] S. Mou, A. D'Arco, L. Tomarchio, S. Macis, A. Curcio, S. Lupi, and M. Petrarca, "Generation of terahertz vector beam bearing tailored topological charge," *APL Photonics* 8, 036103 (2023). <https://doi.org/10.1063/5.0141691>.
- [18] Beresna, M., Gecevičius, M. & Kazansky, P. G. in *Progress in Nonlinear Nano-Optics* (eds Shuji Sakabe, Christoph Lienau, & Rüdiger Grunwald) 31-46 (Springer International Publishing, 2015).
- [19] Z. Jiang, X. G. Xu, and X. C. Zhang, "Improvement of terahertz imaging with a dynamic subtraction technique," *Applied Optics* 39, 2982–2987 (2000).

## Supplementary Information:

### THz complex vortex beam generation theory

The normalized transverse THz polarization vectors  $P_1$  and  $P_2$  generated in a 111-cut Zinc blende crystal by the two balanced pump fields  $E_1$  and  $E_2$ , which have polarization angles of  $\theta$  and  $\theta + 45^\circ$ , respectively, can be written as follows, respectively[16]:

$$P_1 = [\cos 2\theta, -\sin 2\theta] \quad (1)$$

$$P_2 = [-\sin 2\theta, -\cos 2\theta] \quad (2)$$

Where,  $\theta$  is the polarization angle with respect to  $[11\bar{2}]$  axis of the nonlinear crystal. When the  $P_2$  have a phase delay of  $\pi/2$  at THz range with respect to  $P_1$ , the superposition THz field can be written as

$$P = P_1 + iP_2 = P_0[\cos 2\theta - i \sin 2\theta, -\sin 2\theta - i \cos 2\theta]$$

Thus any two pumps linearly polarized with a relative angle of  $45^\circ$  with respect to each other, generate two perpendicular polarized THz signals regardless of the azimuthal angle of  $\theta$ . Instead of two linearly polarized pumps beams, we consider radially/azimuthally polarized (cylinder vortex) pump beams with the azimuthal order of  $l$ . The cylinder vortex pump beams are expressed as  $E_1 = E_0[\cos(l\phi), \sin(l\phi)]$  and  $E_2 = E_0[\cos(l\phi + 45^\circ), \sin(l\phi + 45^\circ)]$ . Where,  $\phi$  is the azimuthal angle.

The superposition THz polarization vector, generated by the two cylinder vortex pump beams with the relative temporal phase delay of  $\pi/2$  will be:

$$P = [\cos(2l\phi) - i \sin(2l\phi), -\sin(2l\phi) - i \cos(2l\phi)] = e^{i(-2l\phi)} [1, -i]$$

It can be seen that the superposition of the THz beam is a **right** circular vortex beam with a spin angular momentum of  $-\hbar$  and an orbit angular momentum of  $-2l\hbar$ .

Consider the same dual cylinder vortex pump beams with a temporal phase difference of  $-\pi/2$ . The generated THz polarization then is:

$$P = [i \cos(2l\phi) - \sin(2l\phi), -i \sin(2l\phi) - \cos(2l\phi)] = e^{i(2l\phi)} [i, -1].$$

This THz beam is a **left** circular vortex beam with a spin angular momentum of  $+\hbar$  and an orbit angular momentum of  $+2l\hbar$ .

Thus the handedness of the spin momentum and the orbit angular momentum were both determined by the phase delay,  $\varphi$ .

Consider the general case of having a phase difference of  $\varphi$ . The THz polarization vector can be written as,

$$P = P_1 + e^{i\varphi} P_2 = [\cos(2l\phi) - e^{i\varphi} \sin(2l\phi), -\sin(2l\phi) - e^{i\varphi} \cos(2l\phi)].$$

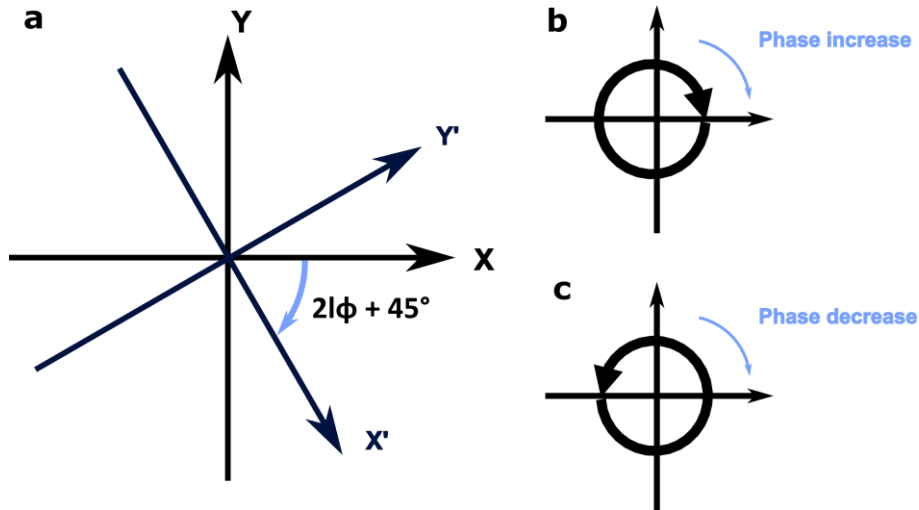


Fig. S1. The coordinate systems transformation (a), and the clockwise phase changes for right-handed circular,  $s = -\hbar$ , (b) and left-handed circular polarization,  $s = +\hbar$  (c).

In order to separate spin and orbital momentum contributions we introduce a local rotating coordinate system  $(X', Y')$  which rotates  $2l\phi + 45^\circ$  clockwise with respect to the fixed laboratory coordinate system  $(X, Y)$ . The generated local THz polarization can be written as,

$$P' = [P_x \cos(2l\phi + 45^\circ) - P_y \sin(2l\phi + 45^\circ), P_x \sin(2l\phi + 45^\circ) + P_y \cos(2l\phi + 45^\circ)] = \frac{\sqrt{2}}{2} [1 + e^{i\varphi}, 1 - e^{i\varphi}],$$

Where  $P_x$  and  $P_y$  are the polarization components along X and Y axis in the laboratory system as shown in Fig. S1. We can further manipulate the expression above:

$$P' = \sqrt{2}e^{i(\varphi/2)} [\cos(\varphi/2), -i\sin(\varphi/2)]$$

It is seen that the local THz field is elliptically polarized with long/short axis aligned along the clockwise rotating coordinate system axis which rotates by  $2l\phi + 45^\circ$ , with respect to the lab coordinate system, and the ellipticity of the local polarization is  $|\tan(\varphi/2)|$ . The fact that in the clockwise rotating coordinate frame the dependence of the polarization vector on the azimuthal angle,  $\phi$ , vanishes shows that the coordinate rotation compensated orbital angular momentum with topological charge  $TC=+2l$ . As shown above the handedness and ellipticity of the local polarization as well as sign of the topological charge of the orbital angular momentum depend on the sign of the phase delay between the pump fields,  $\varphi$ .

For  $\varphi > 0$ , the local elliptical polarization and the orbital angular motion will be right-handed, representing a TC of  $-2l$ . While for  $\varphi < 0$  the local elliptical polarization and the orbital angular motion will be left-handed, representing a TC of  $+2l$ . When the phase delay  $\varphi=0$ , THz beam turns to the cylinder vortex beam with azimuthal phase winding of  $4\pi$ .

In this work, the THz field amplitude and phase were reconstructed using THz polarimetry method, which is done in the fixed *reconstruction coordinate frame* a coordinate frame which is  $45^\circ$  clockwise rotated with respect to the laboratory coordinate system. The SOPs in the **Results** are given in this reconstruction coordinate frame. The THz local polarization vector in this frame is:

$$P = \sqrt{2}e^{i(-sgn(\varphi)2l\phi+\varphi/2)} [\cos(\varphi/2), -i\sin(\varphi/2)].$$



## Methods:

### Transformations of SOPs of the pump and THz beams

According to the local THz polarization expression from **Supplementary Information**, the SOPs of THz field in reconstructed coordinate frame can be plotted on HOP sphere illustrated in Fig. 1. The global THz polarization can be expressed by two orthogonal pure SAM states, carrying opposite OAM to map all the SOPs on HOP sphere.

$$P = \left[ \cos\left(\frac{\varphi}{2} + \frac{\pi}{4}\right) e^{(+i2l\phi - \frac{\pi}{2} - 2\theta)} \right] |L\rangle + \left[ \sin\left(\frac{\varphi}{2} + \frac{\pi}{4}\right) e^{(-i2l\phi - \frac{\pi}{2} - 2\theta)} \right] |R\rangle$$

Two angles  $2\theta$  and  $\varphi$  are introduced to traverse the entire HOP sphere illustrated in Fig. 1, of which  $\theta$  is the rotation angle of S-waveplate and  $\varphi$  is the phase delay between two pumps. The five typical states **a-e** in Fig. 1 represent SOPs with varying phase delay and S-waveplate setting at  $\theta=0^\circ$ . The states **c, f, g** and **h** on the equator represent SOPs with zero phase delay ( $\varphi=0$ ) between two pumps. From state **c**, the other SOPs on the equator are reached by rotating the S-waveplate to manipulate  $\theta$ . States **f-h** correspond to the S-waveplate angles of  $45^\circ$ ,  $90^\circ$  and  $135^\circ$ , respectively. Note that the SOPs in Fig. 1 are shown under the reconstructed coordinate frame OExEy.

The SOP transformation processes of state **c, f, g** and **h** in Fig. 1 from the linearly polarized pumps to CV pumps and further to CV THz beams are shown schematically in Fig. S1, achieved by setting the S-waveplate at  $\theta=0^\circ$ ,  $45^\circ$ ,  $90^\circ$  and  $135^\circ$ . Note that the SOPs in Fig.S1 are plotted under the laboratory coordinate system of OXY. The polarization orientations of two pumps are shown in Fig.S1 (a) and (d), and after the S-waveplate, the SOPs turn to CV pumps in Fig.S1 (b) and (e). The local polarizations of these two CV pumps are  $45^\circ$  with respect to each other. Following the rule described in **Supplementary Information**, the two THz beams generated by the 111-ZnTe are CV beams with perpendicular local polarizations, as shown in Fig. S1(c) and (f). The first row of the superpositioned CV THz beam corresponds to the state **c** in Fig. S1. To achieve the CV beam as depicted in Fig. S1-f, we rotate the S-waveplate and set it at  $\theta=45^\circ$ . The schematical transformation of SOPs in this case is illustrated in the second row of Fig. S1 as a comparison. As we can see, the generated THz CV beams are as depicted in the second row of Fig. S1 (c) and (f), with local polarization rotate  $90^\circ$  compared to that of first row. The third row represents state **g** in Fig. S1, of which the S-waveplate was set at  $90^\circ$ , and the local polarization of CV THz are  $180^\circ$  compared to the State **c**. Similarly, the fourth row represents state **h** with S-waveplate set at  $\theta=135^\circ$ .


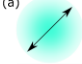
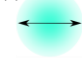


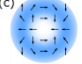


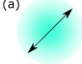
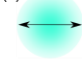


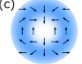
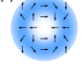

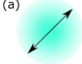
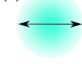


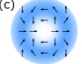
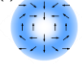

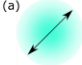
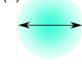
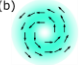

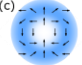
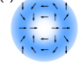
	S-waveplate	Linearly polarized pump	Cylinder vortex pump	Cylinder vortex THz
<b>State c</b>	 $\theta = 0$	<p>pump 1</p>  <p>pump 2</p> 	<p>pump 1</p>  <p>pump 2</p> 	<p>pump 1</p>  <p>pump 2</p> 
<b>State f</b>	 $\theta = 45$	<p>pump 1</p>  <p>pump 2</p> 	<p>pump 1</p>  <p>pump 2</p> 	<p>pump 1</p>  <p>pump 2</p> 
<b>State g</b>	 $\theta = 90$	<p>pump 1</p>  <p>pump 2</p> 	<p>pump 1</p>  <p>pump 2</p> 	<p>pump 1</p>  <p>pump 2</p> 
<b>State h</b>	 $\theta = 135$	<p>pump 1</p>  <p>pump 2</p> 	<p>pump 1</p>  <p>pump 2</p> 	<p>pump 1</p>  <p>pump 2</p> 

Fig. S1. The schematic of SOPs of the two pumps and generated THz beams at waveplate  $\theta=0^\circ$  (state **c**),  $45^\circ$ (state **f**),  $90^\circ$ (state **g**) and  $135^\circ$ (state **h**) in OXY frame. Linearly polarized dual pumps before S-waveplate (a) and (d). SOPs of the cylinder vortex pump beams with  $l=1$  after S-waveplate: (b) is the pump beam (a) after S-waveplate while the (e) was generated from (d). THz vortex beams generated after 111-ZnTe crystal: (c) generated by pump (b), and (d) generated by pump (e).

The intensity distribution of the two pumps after  $0^\circ$  S-waveplate were measured with and without polarizer by a CCD camera, and the measured results are shown in Fig. S2. The measured polarization distributions of pump 1 and pump 2 are aligned with the schematic illustration of state c in Fig. S1.

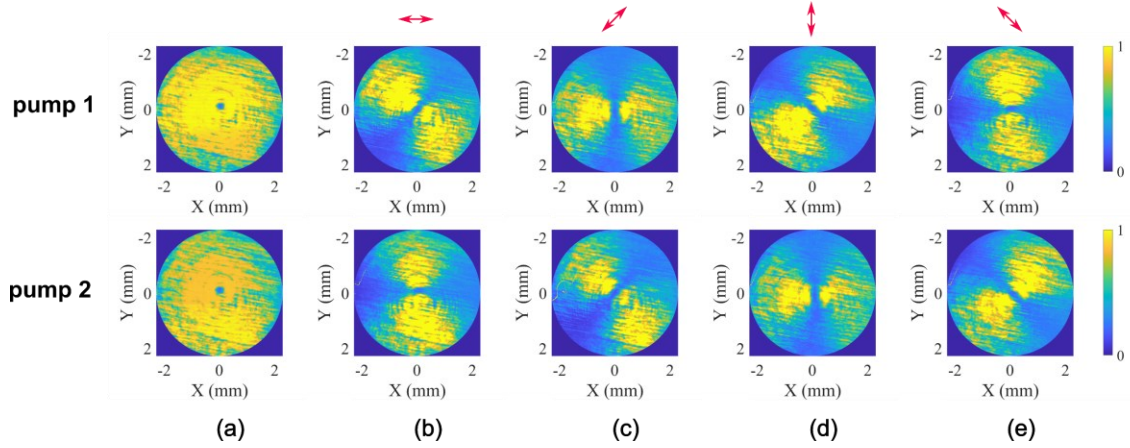


Fig. S2. The intensity distribution of CV pumps after  $0^\circ$  S-waveplate without polarizer (a) and with polarizer (b)-(e). The upper row is results for pump 1, and the bottom row is results for pump 2. Pink arrows: Transmittance orientation of polarizer.

### Zero phase delay calibration

To facilitate this experiment, the zero phase delay between two pump beams was calibrated by employing two delay-lines. First, Pump 2 arm with delay-line was blocked and the temporal THz signal generated by single Pump 1 beam was scanned by controlling the probe beam delay-line. The probe beam delay-line was then fixed at the peak position, and the two pump arms were unblocked at the meanwhile. The THz signal was measured by controlling the delay-line on Pump 2 arm. The delay-line on Pump 2 arm was set as zero phase delay position when THz signal reaches the peak. The S-waveplate was not used in this calibration step.

After inserting S-waveplate and keeping the temporal phase delay at nominal zero, the THz vortices generated by the two pump cylindrical vortices separately and by using both pump beams together with S-waveplate at  $0^\circ$  were experimentally verified and shown in Fig. S3. THz electrical fields generated independently by the cylinder vortex pumps separately are measured with probe delay-line sitting at peak position are shown in Fig. S3(a) and (b). The experimental results are aligned well with the simulated polarization distributions in Fig. S1. Both THz fields exhibit the four-petal pattern, implying cylindrical vortex beam with a polarization rotation of  $4\pi$ . The topological winding number (TC) of the THz vortex polarization singularity is identified as -2 (TC of pump is +1). The local polarizations of two THz vortices are shown in purple arrows in Fig. S3(a) and (b), that are perpendicular to each other at any arbitrary azimuthal angle, representing the orthogonal eigenstates of the cylindrical vortex beam. THz beam generated together by two pump beams with zero phase delay is shown in Fig. S3(c), representing another CV beam with the same topological winding number. This vortex beam is the coherent superposition of the two THz fields in Figs. S3(a) and (b), with local polarization rotated by  $\pi/4$ . The profiles shown in Fig. S3 validate the accuracy of the pump parameters and primarily demonstrate the experimental functionality of the setup. It is noted that results in this figure were measured without the two WGP, so that the SOPs are under laboratory coordinate system. The SOPs of Fig. S3(c) correspond to the beam on equator of the higher-order Poincaré sphere.

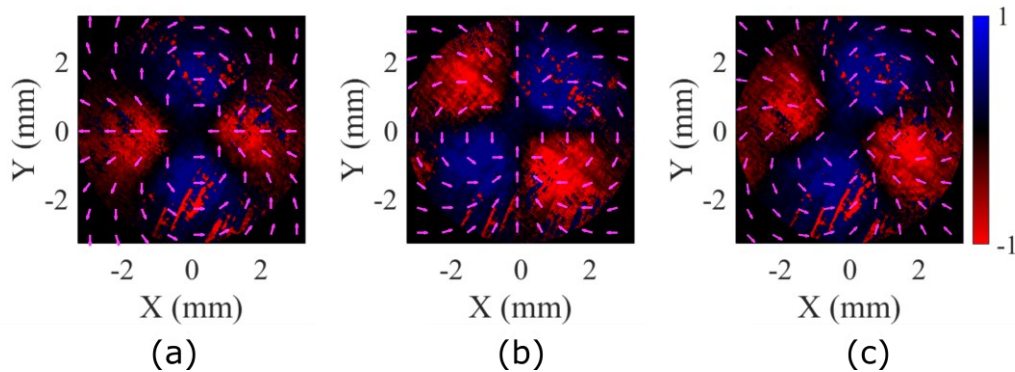
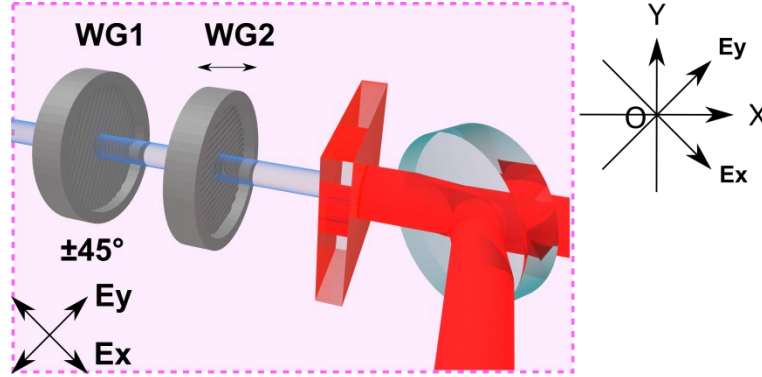


Fig. S3. Electric fields of THz vector vortex. Generated by Pump 1 (a), Pump 2 (b), and Pump 1 plus Pump 2 (c). Purple arrows: polarization orientations.

### THz polarimetry technique

THz polarimetry technique is built by inserting a pair of wire-grid polarizers (WGP) before the detection crystal, as illustrated in Fig. S4. The transmittance orientation of the second WGP (WG2) was aligned with the maximum nonlinearity of the detection crystal (110-cut ZnTe) to guarantee the maximum sensitivity. In this set-up, the second WGP was set at  $0^\circ$  with horizontal transmittance orientation. The first WGP (WG1) was set at  $\pm 45^\circ$  to measure the components  $E_x$  and  $E_y$  of THz electric field, separately. The orientations of  $E_x$  and  $E_y$  (field reconstruction frame) and the laboratory coordinate frames are illustrated in Fig.S4. The THz electric field components were able to be measured without rotating the detection crystal to avoid inconsistency during the measurements.



**Fig. S4.** THz polarimetry setup. WG1, WG2: wire grid polarizer, black arrows: transmittance orientation of wire grid polarizers. OXY and OExEy represent laboratory and reconstruction coordinate frames.